1-1-2007

Robust adaptive control of conjugated polymer actuators

Yang Fang
Michigan State University

Xiaobo Tan
Michigan State University

Gursel Alici
University of Wollongong, gursel@uow.edu.au

Robust Adaptive Control of Conjugated Polymer Actuators

Yang Fang[a], Xiaobo Tan[a], and Gürsel Alici[b]

[a]Smart Microsystems Laboratory, Department of Electrical & Computer Engineering
Michigan State University, East Lansing, MI 48824, USA;
[b]School of Mechanical, Materials, and Mechatronics Engineering
University of Wollongong, 2522 NSW, Australia

ABSTRACT

Conjugated polymers are promising actuation materials for bio and micromanipulation systems, biomimetic robots, and biomedical devices. Sophisticated electrochemomechanical dynamics in these materials, however, poses significant challenges in ensuring their consistent, robust performance in applications. In this paper an effective adaptive control strategy is proposed for conjugated polymer actuators. A self-tuning regulator is designed based on a simple actuator model, which is obtained through reduction of an infinite-dimensional physical model and captures the essential actuation dynamics. The control scheme is made robust against unmodeled dynamics and measurement noises with parameter projection, which forces the parameter estimates to stay within physically-meaningful regions. The robust adaptive control method is applied to a trilayer polypyrrole actuator that demonstrates significant time-varying actuation behavior in air due to the solvent evaporation. Experimental results show that, during four-hour continuous operation, the proposed scheme delivers consistent tracking performance with the normalized tracking error decreasing from 11% to 7%, while the error increases from 7% to 28% and to 50% under a PID controller and a fixed model-following controller, respectively. In the mean time the control effort under the robust adaptive control scheme is much less than that under PID, which is important for prolonging the lifetime of the actuator.

Keywords: Conjugated polymer actuators, polypyrrole (PPy), physical model, model reduction, robust adaptive control.

1. INTRODUCTION

Electroactive polymers (EAPs) are emerging actuation and sensing materials with numerous potential applications in robotics and biomedical systems.[1–4] One class of EAP materials are conjugated polymers, which are also called conducting polymers.[2,5,6] Polypyrrole (PPy) is one of the most commonly used conjugated polymers for actuation purposes. The ions movement during reduction/oxidation (redox) is considered to be the primary mechanism responsible for volumetric change and thus the actuation of conjugated polymers. There has been extensive work on understanding the actuation mechanism of conjugated polymers as well as improving their actuation performance (strain output, strain rate, force output, work per cycle, lifetime, etc.)[2,5–7] However, control and control-oriented modeling of conjugated polymers remain largely unexplored. A proportional controller was used by Qi *et al.* to speed up the transient responses of an polyaniline actuator.[8] P. Madden treated the actuation dynamics as a first-order system and designed a PID controller for a polypyrrole actuator, where his main interest was to demonstrate a feedback loop consisting of polypyrrole actuator and sensor.[9] Taking again a first-order empirical model, Bowers did simulation studies on PID and adaptive control of conjugated polymers, but no experimental results were presented.[10]

The major contribution of this paper is the development of a novel robust adaptive control scheme for conjugated polymer actuators with demonstrated performance in trajectory tracking experiments. A key component of the work is a simple model obtained through model reduction based on a full, infinite-dimensional physical

Further author information: (Send correspondence to Xiaobo Tan.)
Yang Fang: E-mail: fangyang@msu.edu Telephone: 1-517-432-0437
Xiaobo Tan: E-mail: xbtan@msu.edu, Telephone: 1-517-432-5671
Gürsel Alici: E-mail: gursel@uow.edu.au

Electroactive Polymer Actuators and Devices (EAPAD) 2007, edited by Yoseph Bar-Cohen,
Proc. of SPIE Vol. 6524, 652407, (2007) · 0277-786X/07/$18 · doi: 10.1117/12.715755

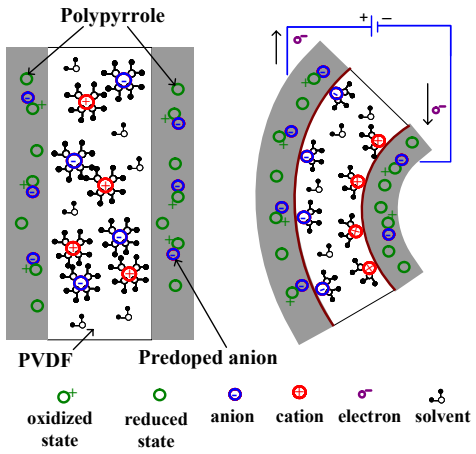

Figure 1. Illustration of the actuation mechanism of trilayer polypyrrole actuator. Left: the sectional view of the trilayer structure; right: bending upon application of a voltage.

model.[11] Thus it captures essential actuation dynamics yet is amenable to efficient real-time control. A recursive least-squares algorithm is then used to identify online the parameters of the reduced model. A self-tuning regulator[12] is designed based on the identified parameters to make the closed-loop system follow a reference model. A parameter projection step ensures that the parameter estimates stay within the physically-meaningful region, and thus makes the system robust against measurement noises, and unmodeled dynamics and nonlinearities.

Tracking experiments are performed to verify the performance of the robust adaptive control scheme. It is shown that, during four-hour continuous operation, the proposed method delivers consistent tracking performance with the normalized tracking error (to be defined precisely later) decreasing from 11% to 7%, while in comparison, the error increases from 7% to 28% and to 50% under a PID controller and a fixed model-following controller, respectively. In the mean time, the control effort required under the adaptive scheme is much less than that under PID, which is important for extending the lifetime of polymer actuators. Furthermore, the evolution of estimated parameters over time agrees with the model prediction when the diffusion constant decreases due to solvent evaporation, which confirms the capability of the reduced model in capturing underlying physics from a different perspective.

The remainder of the paper is organized as follows. The trilayer polypyrrole actuator and its infinite-dimensional physical model are introduced in Section 2. Model reduction is presented in Section 3. In Section 4 the design of robust adaptive controller is described. Experimental results are shown in Section 5. Finally concluding remarks are provided in Section 6.

2. TRILAYER POLYPYRROLE ACTUATOR AND ITS FULL MODEL

2.1. Trilayer Polypyrrole Actuator

The trilayer polypyrrole actuator is illustrated in Fig. 1. It is fabricated by the Intelligent Polymer Research Institute at the University of Wollongong, Australia. In the middle is an amorphous, porous polyvinylidene fluoride (PVDF) layer (110 μm thick) that serves both as a backing material and a storage tank for the electrolyte.[13] The electrolyte used is 0.05 M tetrabutylammonium hexafluorophosphate ($TBA^+PF_6^-$) in the solvent propylene carbonate (PC). On both sides of the actuator are the polypyrrole layers (30 μm each). During the electrochemical deposition of these layers, the anions PF_6^- were introduced into the polymer matrix (a process called *doping*). When a voltage is applied across the actuator, the polypyrrole layer on the anode side is oxidized and absorbs anions while that on the cathode side is reduced and gives up anions. This causes expansion of the oxidized layer and contraction of the reduced layer, resulting in a bending motion.

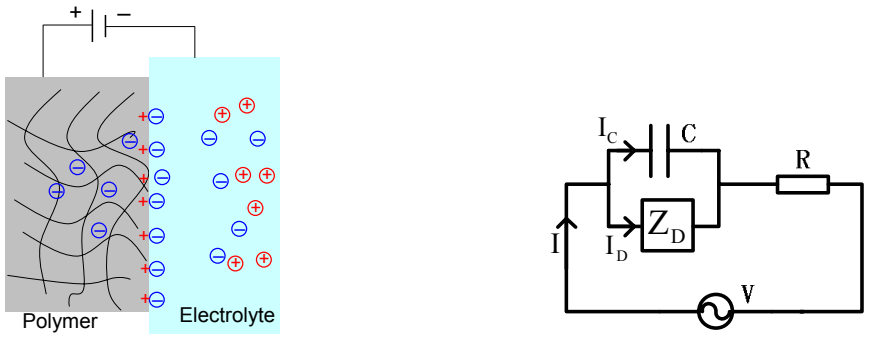

Figure 2. (a) Illustration of double-layer charging and diffusion for a conjugated polymer film with one side in contact with electrolyte; (b) equivalent circuit model for the polymer impedance.

2.2. Electrochemomechanical Model of Trilayer PPy Actuator

The electrochemomechanical model consists of three modules: 1) the electrical admittance module; 2) the electromechanical coupling module ; and 3) the mechanical module.

2.2.1. Electrical Admittance Module

Consider a conjugated polymer film in contact with an electrolyte, as shown in Fig. 2(a). This represents, for instance, one polypyrrole layer in contact with the electrolyte-containing PVDF layer in the case of trilayer PPy actuator. When a positive potential is applied to the polymer, the anions in the electrolyte migrate toward the polymer, which results in double-layer charges at the polymer/electrolyte interface. J. Madden thus proposed a diffusive-elastic-metal model for polypyrrole, where it was assumed that the polymer matrix is perfectly conducting and the ion transport within the polymer is solely determined by diffusion.[11] The admittance model showed good agreement with experimental data over a wide range of frequencies,[11] and thus will be adopted in this paper.

Fig. 2 (b) shows an equivalent circuit model of the polymer impedance, where C denotes the double-layer capacitance at the polymer/electrolyte interface and R is the electrolyte and contact resistance. Z_D represents the "diffusion impedance", which will be clarified in the derivation below. In the Laplace domain the total current $I(s)$ in the circuit is the sum of the double-layer charging current $I_C(s)$ and the current $I_D(s)$ diffusing into polymer:

$$I(s) = I_C(s) + I_D(s). \tag{1}$$

The Kirchhoff's voltage law gives

$$V(s) = I(s) \cdot R + \frac{1}{s \cdot C} \cdot I_C(s). \tag{2}$$

Let x denote the thickness direction of the polymer, with $x = 0$ representing the polymer/electrolyte interface. Assume that the ion concentration varies only in the x-direction, which will be denoted as $c(x, s)$. From Fick's law of diffusion, one has

$$I_D(s) = -F \cdot A \cdot D \cdot \frac{\partial c}{\partial x}(x, s)|_{x=0}, \tag{3}$$

where A is the surface area of the polymer, F is the Faraday constant, D is the diffusion coefficient, and $\frac{\partial c}{\partial x}(x, s)|_{x=0}$ represents the gradient of ion concentration at the interface. Assume that the thickness of double-layer is δ and that the ion concentration within the double-layer is uniform, which equals $c(0, s)$. It follows that

$$I_C(s) = s \cdot Q_C(s) = F \cdot A \cdot \delta \cdot s \cdot c(0, s). \tag{4}$$

The last equation needed for the derivation is the diffusion equation, which reads in the time domain:

$$\frac{\partial c}{\partial t} = D \frac{\partial^2 c}{\partial x^2}, \quad 0 < x < h, \tag{5}$$

where h is the thickness of the polymer layer.

J. Madden used separation of variables to solve the concentration profile in response to a step change of concentration at the interface, and then used convolution of the step response with a given concentration gradient at the boundary to obtain $c(x,t)$.[11] A more straightforward derivation is given here, which first transforms the diffusion equation (5) into the Laplace domain:

$$\frac{\partial^2 c(x,s)}{\partial x^2} = \frac{s}{D} \cdot c(x,s). \tag{6}$$

Eq. (6) has a generic solution of the form

$$c(x,s) = C_1(s)e^{-\sqrt{s/D}\ x} + C_2(s)e^{\sqrt{s/D}\ x}. \tag{7}$$

Letting $x = 0$ in (7) and using (4), one gets

$$C_1(s) + C_2(s) = \frac{I_C(s)}{F \cdot A \cdot \delta \cdot s}. \tag{8}$$

From (3) and (7), one has

$$-\sqrt{\frac{s}{D}}C_1(s) + \sqrt{\frac{s}{D}}C_2(s) = -\frac{I_D(s)}{F \cdot A \cdot D}. \tag{9}$$

For the trilayer polypyrrole actuator, there is no ionic flux at the other surface of the polypyrrole layer, which gives the boundary condition at $x = h$:

$$\frac{\partial c(x,s)}{\partial x}|_{x=h} = -\sqrt{\frac{s}{D}}C_1(s)e^{-\sqrt{s/D}\ h} + \sqrt{\frac{s}{D}}C_2(s)e^{\sqrt{s/D}\ h} = 0. \tag{10}$$

From (3), (4), (8), (9) and (10), $I_C(s)$ and $I_D(s)$ can be written in terms of $V(s)$ and $I(s)$:

$$I_C(s) = s \cdot C \cdot (V(s) - I(s) \cdot R), \tag{11}$$

$$I_D(s) = I(s) - s \cdot C \cdot (V(s) - I(s) \cdot R). \tag{12}$$

Note that the voltage input $V(s)$ is applied across two double-layers and therefore the total admittance $Y(s)$ is half of the admittance of the single layer. From (1), (11) and (12), one gets

$$Y(s) = \frac{1}{2} \cdot \frac{s[\frac{\sqrt{D}}{\delta}\tanh(h\sqrt{s/D}) + \sqrt{s}\,]}{\frac{\sqrt{s}}{C} + R \cdot s^{3/2} + R \cdot \frac{\sqrt{D}}{\delta} \cdot s \cdot \tanh(h\sqrt{s/D})}. \tag{13}$$

2.2.2. Electromechanical coupling

The anions transferred to the polymer cause expansion of the polymer. It was shown that the induced in-plane strain ϵ is proportional to the density ρ of the transferred charges[14] :

$$\epsilon = \alpha\rho, \tag{14}$$

where α is the strain-to-charge ratio. Equivalently, the induced stress by the transferred charges is

$$\sigma = \alpha E_{ppy}\rho, \tag{15}$$

where E_{ppy} denotes the Young's modulus of the polypyrrole layer.

Since the bulk capacitance of the polymer is much larger than the double-layer capacitance, the charges stored in the double layer at the steady state is negligible compared to that in the bulk.[9] Consequently one can obtain the density $\rho(s)$ by

$$\rho(s) = \frac{I(s)}{sWLh}, \tag{16}$$

where W, L are the width and the length of the polypyrrole layer, respectively.

2.2.3. Mechanical Output

Consider a trilayer actuator clamped at one end, as shown in Fig. 3. It can be shown through moment balance that the (uniform) beam curvature κ under the induced stress (15) and in the absence of external force is[9]

$$\kappa = \frac{3\alpha}{2h_{pvdf}} \cdot \frac{(1+\frac{h}{h_{pvdf}})^2 - 1}{(1+\frac{h}{h_{pvdf}})^3 + \frac{E_{pvdf}}{E_{ppy}} - 1} \cdot \rho, \tag{17}$$

where E_{pvdf} is the Young's modulus of the PVDF layer, and h_{pvdf} denotes half of its thickness.

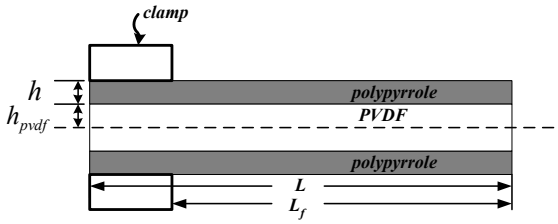

Figure 3. Geometry of the trilayer actuator.

In experiments the beam tip displacement is measured by a laser distance sensor, as illustrated in Fig. 4. One can relate the measured displacement $y = d_0 - d$ to the curvature κ via simple geometric calculations. For small bending ($y << l$), the curvature is approximately linear with respect to the displacement:

$$\kappa = \frac{1}{r} \approx \frac{2y}{l^2}. \tag{18}$$

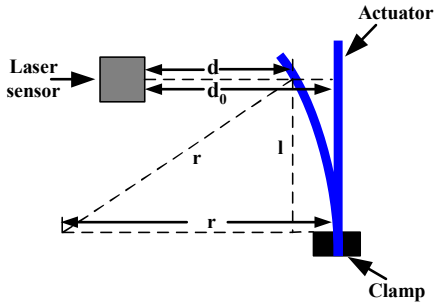

Figure 4. Geometric relationship between the beam curvature and the tip displacement.

Combining (13), (16), (17), and (18), one obtains the transfer function from the voltage input $V(s)$ to the bending displacement output $y(s)$:

$$\frac{y(s)}{V(s)} = C_m \frac{\frac{\sqrt{D}}{\delta}\tanh(h\sqrt{\frac{s}{D}}) + \sqrt{s}}{\frac{\sqrt{s}}{C} + R \cdot s^{3/2} + R \cdot \frac{\sqrt{D}}{\delta} \cdot s \cdot \tanh(h\sqrt{\frac{s}{D}})}, \tag{19}$$

with the constant

$$C_m \triangleq \frac{3\alpha l^2[(1+\frac{h}{h_{pvdf}})^2 - 1]}{8h_{pvdf}hWL[(1+\frac{h}{h_{pvdf}})^3 + \frac{E_{pvdf}}{E_{ppy}} - 1]}.$$

3. MODEL REDUCTION

Utilizing the equality[11]

$$\frac{\tanh(\frac{1}{2}\sqrt{\frac{s}{z}})}{4\sqrt{sz}} = \sum_{n=0}^{\infty} \frac{1}{s+\pi^2(2n+1)^2 z}$$

and letting $z = \frac{D}{4h^2}$, the full electrochemomechanical model (19) can be rewritten as

$$\frac{y(s)}{V(s)} = \frac{C_m}{sR + \frac{1}{C(1+\frac{2D}{h\delta}\sum_{n=0}^{\infty}\frac{1}{s+\pi^2(2n+1)^2 D(2h)^{-2}})}}. \tag{20}$$

However, this is an infinite-dimensional system, which is not suitable for real-time control purposes.

To understand the rationale behind model reduction, take typical parameters $D = 2\times 10^{-10}$ m^2/s and $h = 30$ μm. The constant $\pi^2 D(2h)^{-2} = 0.548$. The pole of $\frac{1}{s+\pi^2(2n+1)^2 D(2h)^{-2}}$ is at -13.7 for $n = 2$, at -26.9 for $n = 3$, and at -44.4 for $n = 4$, etc. This indicates that one can obtain a low-order approximation to (20) by ignoring terms associated with large n. In particular, for a low-frequency input, the approximation will preserve well the behavior of (20)*.

We thus discard terms with $n \geq 2$. This results in the following third-order system for the actuator:

$$\frac{y(s)}{V(s)} = \frac{b_1' s^2 + b_2' s + b_3'}{s^3 + a_1' s^2 + a_2' s + a_3'}, \tag{21}$$

where the parameters all have explicit physical meanings:

$$a_1' = \frac{4D}{h\delta} + \frac{5\pi^2 D}{2h^2} + \frac{1}{RC}, \quad a_2' = \frac{5\pi^2 D^2}{h^3\delta} + \frac{9\pi^4 D^2}{16h^4} + \frac{5\pi^2 D}{2h^2 RC}, \quad a_3' = \frac{9\pi^4 D^2}{16h^4 RC},$$
$$b_1' = \frac{C_m}{R}, \quad b_2' = \frac{4DC_m}{h\delta R} + \frac{5\pi^2 DC_m}{2h^2 R}, \quad b_3' = \frac{5\pi^2 D^2 C_m}{h^3\delta R} + \frac{9\pi^4 D^2 C_m}{16h^4 R}.$$

The system (21) has three poles with explicit expressions:[15]

$$p_1 = 2\sqrt{-Q}\cos(\frac{\theta}{3}) - \frac{1}{3}a_1' \tag{22}$$
$$p_2 = 2\sqrt{-Q}\cos(\frac{\theta+2\pi}{3}) - \frac{1}{3}a_1', \tag{23}$$
$$p_3 = 2\sqrt{-Q}\cos(\frac{\theta+4\pi}{3}) - \frac{1}{3}a_1', \tag{24}$$

where

$$\theta = \cos^{-1}(\frac{P}{\sqrt{-Q^3}}), \quad Q = \frac{3a_2' - a_1'^2}{9}, \quad P = \frac{9a_1'a_2' - 27a_3' - 2a_1'^3}{54}.$$

With typical physical parameters, a_1', a_2', and a_3' are all relatively large numbers ($>> 1$). This implies $a_1'^2 >> 3a_2'$ in Q, and $2a_1'^3 >> 9a_1'a_2'$ and $2a_1'^3 >> 27a_3'$ in P, which leads to

$$Q \approx -\frac{a_1'^2}{9}, \quad P \approx -\frac{a_1'^3}{27}, \quad \sqrt{-Q} \approx \frac{a_1'}{3},$$
$$\theta \approx \cos^{-1}(-\frac{a_1'^3/27}{\sqrt{a_1'^6/9^3}}) = \cos^{-1}(-1) = \pi.$$

*It turns out that this will also provide a good approximation to the original dynamics at *very* high frequencies since then both models will behave like $\frac{CC_m}{1+sRC}$.

The poles (22) through (24) are thus approximately

$$p_1 \approx 0, \qquad p_2 \approx -a_1', \qquad p_3 \approx 0. \tag{25}$$

Clearly $|p_2|$ is very large while $|p_1|$ and $|p_3|$ are relatively small.

The analysis on the zeros is simpler. The zeros of (21) are

$$z_1 = \frac{-b_2' - \sqrt{b_2'^2 - 4 \cdot b_1' \cdot b_3'}}{2b_1'}, \qquad z_2 = \frac{-b_2' + \sqrt{b_2'^2 - 4 \cdot b_1' \cdot b_3'}}{2b_1'}. \tag{26}$$

With typical parameters, $4 \cdot b_1' \cdot b_3' \ll b_2'^2$, $b_2 \gg b_1$, which implies

$$z_1 \approx -\frac{b_2'}{b_1'}, \qquad z_2 \approx 0. \tag{27}$$

Therefore, $|z_1|$ is very large while $|z_2|$ is relatively small. Thus one can safely ignore one pole and one zero of (21).[16] The final reduced model for the trilayer actuator therefore has the following structure:

$$\frac{y(s)}{V(s)} = \frac{b_1 s + b_2}{s^2 + a_1 s + a_2}. \tag{28}$$

Eq. (28) captures the dominant physics of the actuator within the actuation bandwidth. In particular, all parameters of (28) can be related to fundamental physical parameters for the full model (19).

4. DESIGN OF ROBUST ADAPTIVE CONTROLLER

4.1. Self-Tuning Regulator

Controller adaptation is desirable for conjugated polymers since their actuation behaviors can vary significantly over time. In this paper a self-tuning regulator is adopted due to its simplicity. The idea is to estimate the system parameters online, then construct a controller based on these estimates so that the closed-loop system would behave like a model system $G_m(s)$ (*model-following*). Fig. 5 illustrates the components of a self-tuning regulator.

Based on (28), let the model system be

$$G_m(s) = \frac{b_{1m} s + b_{2m}}{s^2 + a_{1m} s + a_{2m}}.$$

Let the reference input be $r(s)$ in the Laplace domain. The goal of model-following is to compute the input $V(s)$ to (28) so that the output $y(s)$ follows $y_m(s) = G_m(s) r(s)$. Given the parameters, a_i, b_i, $i = 1, 2$, the following controller can be found through pole-placement design:[12]

$$V(s) = \frac{b_{1m} s + b_{2m}}{b_1 s + b_2} r(s) - \frac{(a_{1m} - a_1) s + (a_{2m} - a_2)}{b_1 s + b_2} y(s). \tag{29}$$

One can verify that the closed-loop system with the controller (29) has transfer function $G_m(s)$.

When the parameters a_i, b_i, $i = 1, 2$ are unknown or slowly time-varying, the controller (29) is constructed based on their estimates $\hat{a}_i$, $\hat{b}_i$, $i = 1, 2$, obtained through a recursive least-squares algorithm

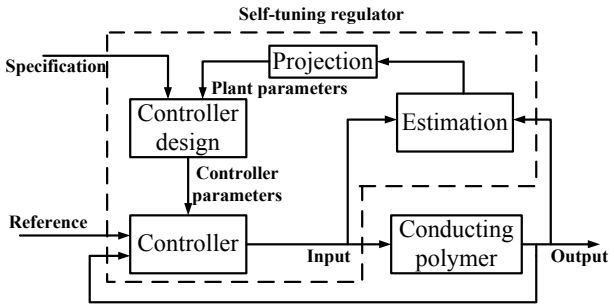

Figure 5. Illustration of the robust self-tuning regulator.

4.2. Parameter Projection

In this paper parameter projection is adopted as a robustification mechanism for the self-tuning regulator against unmodeled higher-frequency dynamics, nonlinearities and noises. In particular, since the two poles and the zero of (28) are all negative, the parameters a_1, a_2, b_1, and b_2 should all be positive. Furthermore, an upper bound $M > 0$ of these parameters can be determined based on the knowledge of physical parameters. Pick a small constant $m > 0$. The projection step is implemented (in discrete time) as follows: for any parameter estimate $\hat{\theta} \in \{\hat{a}_1, \hat{a}_2, \hat{b}_1, \hat{b}_2\}$,

$$\hat{\theta}'(t) = Proj(\hat{\theta}(t)) = \begin{cases} \hat{\theta}(t) & \text{if } m \le \hat{\theta}(t) \le M \\ M & \text{if } \hat{\theta}(t) > M \\ m & \text{if } \hat{\theta}(t) < m \end{cases}, \tag{30}$$

where $\hat{\theta}(t)$ is the estimate from the recursive estimation algorithm, while $\hat{\theta}'(t)$ is the value adopted. In the experiments the values of M and m are chosen to be $M = 1 \times 10^4$, and $m = 0.001$.

It can be shown[17] that the proposed adaptive control scheme in Section 4.1 with parameter projection (30) is robust in the presence of the unmodeled dynamics and nonlinearities, measurement noise, and slow and bounded parameter variations; in particular, all signals in the closed-loop system will be bounded.

5. EXPERIMENTAL RESULTS

Tracking experiments are conducted to examine the effectiveness of the proposed robust adaptive control scheme. A trilayer polypyrrole actuator ($20 \times 5 \times 0.17$ mm) is clamped at one end, where the actuation voltage is applied. The tip displacement is measured by a laser sensor with resolution of 5 μm. The controller is implemented in a PC equipped with dSPACE DS1104. Before each experiment, an actuator cut with the specified size is soaked in the electrolyte ($TBA^+PF_6^-$ in propylene carbonate). The inner porous PVDF layer thus stores electrolyte.

For comparison purposes, a PID controller and a fixed model-following controller are also implemented. Actuators with same dimensions and same conditions are used for all three controllers. The design of the PID controller and the model-following controller is also based on the model structure (28), while the model parameters are identified in separate experiments shortly before the tracking experiment starts. The parameters of the PID controller and the model-following controller remain constant throughout each experiment. The reference model $G_m(s)$ is chosen to be

$$G_m(s) = \frac{s + 1.5}{s^2 + 4s + 4}.$$

The reference input in experiments is chosen as $r(t) = 0.5\sin(\pi t) + 0.5\sin(0.2\pi t)$, and the actuator output $y(t)$ is required to track the desired trajectory $y_m(t) = G_m(s)[r(\cdot)](t)$. The latter contains two frequency components (0.1 Hz and 0.5 Hz) with a peak-to-peak variation of 0.62 mm. Each experiment runs continuously for four hours. Fig. 6 shows the tracking results at the beginning of the experiment ($t = 0$ h), while Fig. 7 shows the results when approaching the end of the experiment ($t = 4$ h).

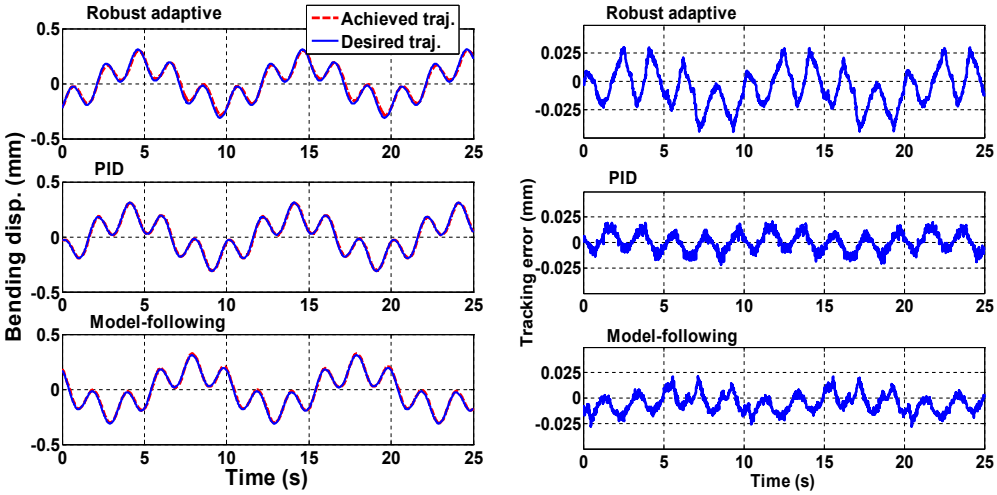

(a) (b)

Figure 6. Experimental results on trajectory tracking, $t = 0$ h. (a) Achieved trajectories versus desired one under the three controllers; (b) instantaneous tracking errors under the three schemes.

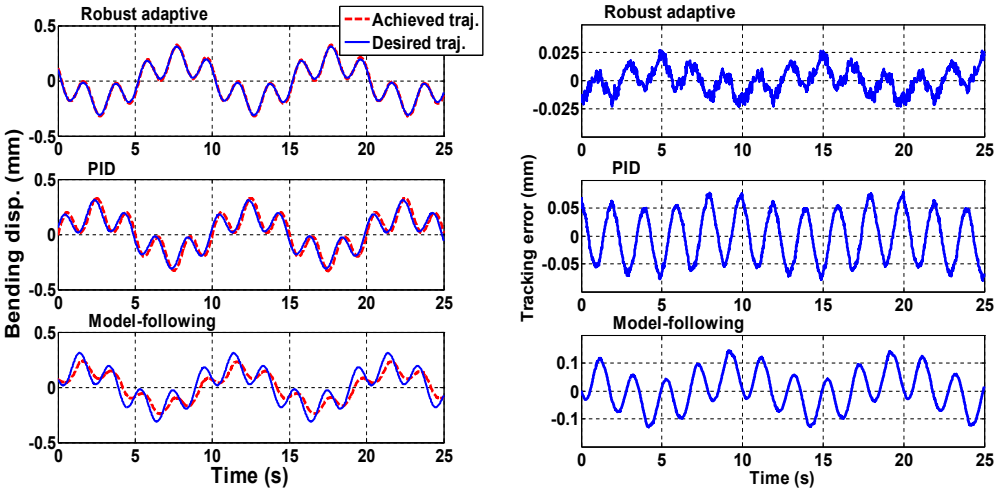

(a) (b)

Figure 7. Experimental results on trajectory tracking, $t = 4$ h. (a) Achieved trajectories versus desired one under the three controllers; (b) instantaneous tracking errors under the three schemes.

Given a starting time t_0 and a constant $T > 0$, we define the *normalized average error* e_a and the *normalized maximum error* e_m for each tracking experiment:

$$e_a \triangleq \frac{\int_{t_0}^{t_0+T} |y(t) - y_m(t)|dt}{\int_{t_0}^{t_0+T} |y_m(t)|dt}, \quad e_m \triangleq \frac{\max_{t\in[t_0,t_0+T]} |y(t) - y_m(t)|}{\max_{t\in[t_0,t_0+T]} |y_m(t)|},$$

which characterize the average and the instantaneous tracking performance during $[t_0, t_0 + T]$, respectively. Throughout this paper, T is chosen to be 100 s. Under the robust adaptive scheme, e_a drops from 11% at $t_0 = 0$ h to 7% at $t = 4$ h, and e_m drops from 15% to 9% for the same period. In comparison, e_a increases from 7% to 28% under the PID controller, from 7% to 50% under the fixed model-following controller, and e_m

increases from 8% to 25% under the PID scheme, and from 10% to 48% under the model-following scheme. Fig. 8 shows the evolution of e_a and e_m, measured and calculated every half a hour, under the three schemes. It is clear that the robust adaptive control scheme delivers consistent tracking performance during the four-hour continuous operation, while the tracking performance under the PID scheme or the fixed model-following scheme deteriorates over time.

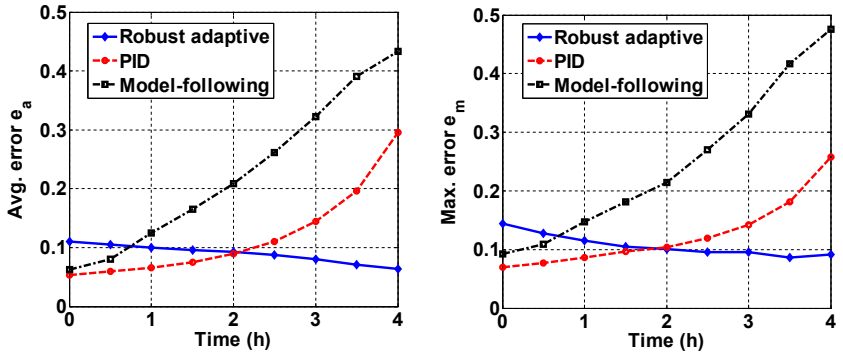

(a) (b)

Figure 8. Normalized average error e_a and maximum error e_m under the three control schemes. (a) Evolution of e_a; (b) evolution of e_m.

It is also important to compare the control efforts required under the different control schemes. Low control effort is highly desirable since that leads to long working life for the conjugated polymer actuator. Fig. 9 shows the evolution of the magnitude of voltage input under each scheme. The required voltage increases over time under every scheme, which is due to the deteriorating actuation capability of the actuator as the solvent evaporates. However, it can be clearly seen that the voltage input under the adaptive scheme is much lower than that under the PID scheme, and also lower than that under the model-following scheme most of the time.

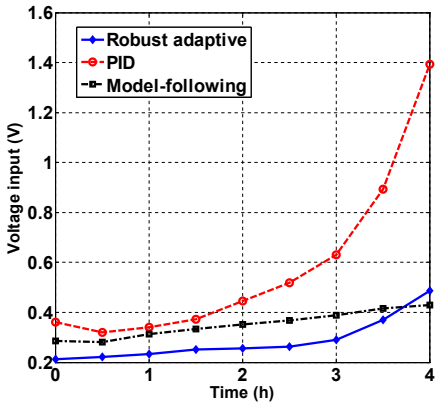

Figure 9. Evolution of voltage input magnitude under the three schemes.

There is another interesting observation during the experiments that supports the validity of the reduced model. The effect of solvent evaporation can be incorporated by taking the diffusion coefficient $D \to 0$. This leads to $p_1 \to 0$, $p_3 \to 0$, and $z_2 \to 0$, where p_1, p_3, and z_2 are the poles and the zero of the reduced model (28), as defined by (22), (24), and (27). Fig. 10 shows the evolution of the poles and the zero in the experiment utilizing the robust adaptive control scheme. It can be seen that they all tend to 0, as predicted by the model.

In previous experiments, the reference inputs used contain two frequency components and are thus persistently

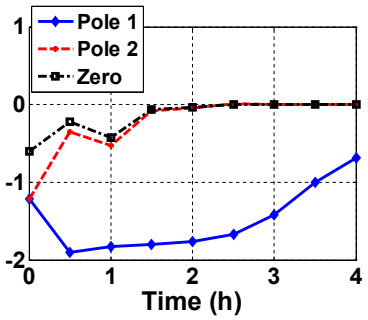

Figure 10. Identified poles and zero in experiment using the robust adaptive control scheme.

exciting of order 4.[12] This is a necessary and sufficient condition for correctly identifying the four parameters in (28). In practice, however, the persistent excitation condition may not always hold, and it is of interest to know whether the robust adaptive scheme still works well in that case. Fig. 11 shows the tracking results under the robust adaptive controller at the beginning and the end of four-hour continuous operation, where the reference input $r(t) = 2\sin(\pi t)$ is persistently exciting only of order 2. The results indicate that the proposed scheme is capable of tracking a non-persistently exciting signal.

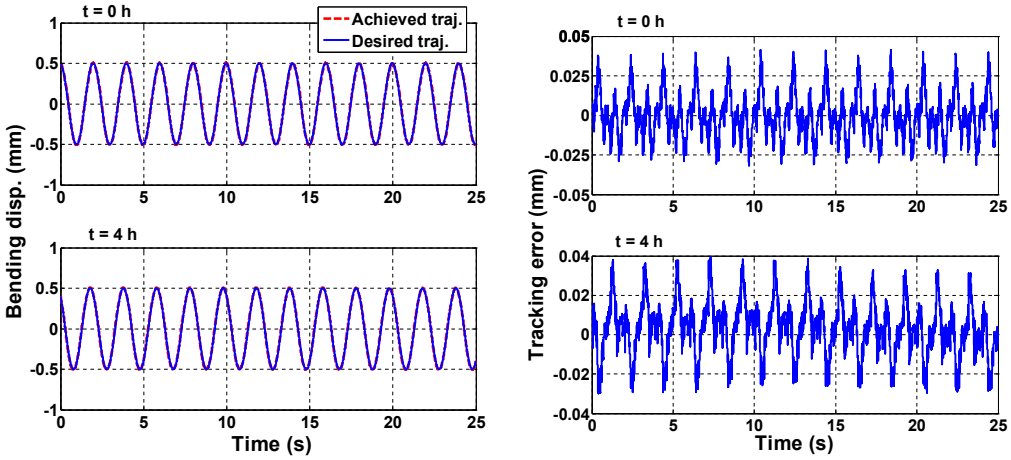

(a) (b)

Figure 11. Experimental results of tracking a non-persistently exciting signal under the robust adaptive controller. (a) Trajectory tracking at $t = 0$ h and $t = 4$ h; (b) Tracking errors at $t = 0$ h and $t = 4$ h.

6. CONCLUSIONS

In this paper a robust adaptive control scheme has been presented for conjugated polymer actuators. The key to the success of this method is a simple actuator model that is reduced from the full, infinite-dimensional physical model. Model reduction is based on the knowledge of the actuation bandwidth as well as typical values of the physical parameters. The reduced model captures relevant actuation physics while enabling simple controller design and implementation. The parameter projection step in the self-tuning regulator ensures the stability of the closed-loop system in the presence of noises and unmodeled dynamics. Experimental results have shown that the proposed scheme is superior to the commonly used PID scheme and to the fixed model-following scheme in terms of both tracking accuracy and required control effort.

The proposed scheme is not restricted to the trilayer polypyrrole actuator although the latter has been used as an example throughout this paper. The model structure applies to other conjugated polymers as well as

other actuator configurations (such as bilayer or linear actuators). Note that the tracking error under the robust adaptive control scheme does not converge to zero, which is due to unmodeled dynamics and nonlinearities, and measurement noises. The impact of unmodeled dynamics can be alleviated by keeping more terms of the series in (20) during model reduction. The effects of nonlinearities (e.g., hysteresis, and oxidation level-dependent material properties) can be modeled and compensated for with a more complex controller design.

ACKNOWLEDGMENTS

This work was supported in part by an NSF CAREER grant (ECS 0547131) and by MSU IRGP (05-IRGP-418).

REFERENCES

1. Y. Bar-Cohen, ed., *Electroactive Polymer (EAP) Actuators as Artificial Muscles: Reality, Potential, and Challenges*, (Bellingham, WA), SPIE–The International Society for Optical Engineering, 2001.
2. E. Smela, "Conjugated polymer actuators for biomedical applications," *Journal of Advanced Materials* **15**(6), pp. 481–494, 2003.
3. M. Shahinpoor and K. J. Kim, "Ionic polymer-metal composites: IV. industrial and medical applications," *Smart Materials and Structures* **14**, pp. 197–214, 2005.
4. F. Carpi and D. De Rossi, "Electroactive polymer-based devices for e-textiles in biomedicine," *IEEE Transactions on Information Technology in Biomedicine* **9**(3), pp. 295–318, 2005.
5. R. Baughman, "Conducting polymer artificial muscles," *Synthetic Metals* **78**, pp. 339–353, 1996.
6. G. G. Wallace, G. M. Spinks, L. Kane-Maguire, and P. R. Teasdale, *Conductive Electroactive Polymers: Intelligent Materials Systems (2nd Edition)*, CRC Press LLC, Boca Raton, FL, 2003.
7. P. G. A. Madden, J. D. W. Madden, P. A. Anquetil, N. A. Vandesteeg, and I. W. Hunter, "The relation of conducting polymer actuator material properties to performance," *IEEE Journal of Oceanic Engineering* **29**, pp. 696–705, 2004.
8. B. Qi, W. Lu, and B. R. Mattes, "Control system for conducting polymer actuators," in *Smart Structures and Materials 2002: Electroactive Polymer Actuators and Devices (EAPAD)*, Y. Bar-Cohen, ed., pp. 359–366, SPIE - The International Society for Optical Engineering, (Bellingham, WA), 2002.
9. P. G. A. Madden, *Development and Modeling of Conducting Polymer Actuators and the Fabrication of a Conducting Polymer Based Feedback Loop*. Phd thesis, Massachusetts Institute of Technology, 2003.
10. T. A. Bowers, "Modeling, simulation, and control of a polypyrrole-based conducting polymer actuator," Master's thesis, Massachusetts Institute of Technology, 2004.
11. J. D. W. Madden, *Conducting Polymer Actuators*. Phd thesis, Massachusetts Institute of Technology, 2000.
12. K. J. Astrom and B. Wittenmark, *Adaptive Control*, Addison-Wesley, 2nd ed., 1995.
13. Y. Wu, G. Alici, G. M. Spinks, and G. G. Wallace, "Fast trilayer polypyrrole bending actuators for high speed applications," *Synthetic Metals* **156**, pp. 1017–1022, 2006.
14. T. F. Otero and J. M. Sansinena, "Bilayer dimensions and movement in artificial muscles," *Bioelectrochemistry and Bioenergetics* **42**(2), pp. 117–122, 1997.
15. W. Dunham, *Journey Through Genius: The Great Theorems of Mathematics*, John Wiley & Sons Inc., 1990.
16. G. F. Franklin, J. D. Powell, and A. Emami-Naeini, *Feedback Control of Dynamic Systems*, Pearson Education, Inc., Upper Saddle River, NJ, 5th ed., 2006.
17. S. M. Naik, P. R. Kumar, and B. E. Ydstie, "Robust continuous-time adaptive control by parameter projection," *IEEE Transaction on Automatic Control* **37**(2), pp. 182–197, 1992.